HHS Public Access

Author manuscript

Int J Rock Mech Min Sci (1997). Author manuscript; available in PMC 2015 September 23.

Published in final edited form as:

Int J Rock Mech Min Sci (1997). 2013 February ; 58: 73–84.

Modelling blast induced damage from a fully coupled explosive charge

Italo A. Onederra[a,*], **Jason K. Furtney**[b], **Ewan Sellers**[c], and **Stephen Iverson**[d]

[a]The University of Queensland, WH Bryan Mining and Geology Research Centre, Australia

[b]Itasca Consulting Group, Inc., Minneapolis, MN, USA

[c]African Explosives Limited, Modderfontein, South Africa

[d]National Institute for Occupational Safety and Health, USA

Abstract

This paper presents one of the latest developments in the blasting engineering modelling field—the Hybrid Stress Blasting Model (HSBM). HSBM includes a rock breakage engine to model detonation, wave propagation, rock fragmentation, and muck pile formation. Results from two controlled blasting experiments were used to evaluate the code's ability to predict the extent of damage. Results indicate that the code is capable of adequately predicting both the extent and shape of the damage zone associated with the influence of point-of-initiation and free-face boundary conditions. Radial fractures extending towards a free face are apparent in the modelling output and matched those mapped after the experiment. In the stage 2 validation experiment, the maximum extent of visible damage was of the order of 1.45 m for the fully coupled 38-mm emulsion charge. Peak radial velocities were predicted within a relative difference of only 1.59% at the nearest history point at 0.3 m from the explosive charge. Discrepancies were larger further away from the charge, with relative differences of −22.4% and −42.9% at distances of 0.46 m and 0.61 m, respectively, meaning that the model overestimated particle velocities at these distances. This attenuation deficiency in the modelling produced an overestimation of the damage zone at the corner of the block due to excessive stress reflections. The extent of visible damage in the immediate vicinity of the blasthole adequately matched the measurements.

Keywords

Blast damage; Blast modelling; Damage modelling; Blasting; Rock breakage; Rock; Fragmentation

*Corresponding author. Current address: CRC Mining, Pinjarra Hills, Building 102-2436 Moggill Rd, Brisbane, QLD 4069, Australia. Tel.: +61 7 3365 5623; Mob.: +61 408 133 324; fax: +61 7 3365 5636. i.onederra@uq.edu.au, i.onederra@crcmining.com.au (I.A. Onederra).

9. Disclaimer

The findings and conclusions in this paper are those of the authors and do not necessarily represent the views of the National Institute for Occupational Safety and Health (NIOSH). Mentioning any company name, product or software does not constitute endorsement by NIOSH.

1. Introduction

Blasting in the mining industry is being transformed and can no longer be treated as an art form or a practice purely dependent upon experiences of individual miners. Examples of key drivers that have demanded consistent and more accurate blast results are initiatives to control pit wall damage to help mine steeper pit slope angles, to control damage to underground excavation boundaries during tunnel development and stope mining, and to reduce reinforcement requirements and minimise local instabilities and dilution.

Over the years there have been significant developments in computational mechanics of both continua and discontinua [1,2]. With advances in computer hardware, computational mechanics of discontinua has emerged as an important and fast growing field of computational mechanics with applications in many industrial scale problems including rock blasting and mining [3]. After a detailed review of computational methods available to model the rock blasting process, a consortium of companies acknowledged the need to develop an advanced modelling tool that was able to consider explosive detonation, initial shock, fracturing, damage, fragmentation, and rock mass movement [4]. The main objective was to develop a tool that could be used as a “virtual” blasting laboratory. Designated as the Hybrid Stress Blasting Model (HSBM), this project has involved principal researchers and consultants from the University of Queensland, Itasca Consulting group, and UK-based detonation experts from academia including Cambridge, Imperial, and Leeds Universities. The project has also collaborated and shared experiences with external institutes such as the National Institute for Occupational Safety and Health (NIOSH) in Spokane, Washington, USA.

This paper gives a brief description of the HSBM and documents the results of calibration and evaluation tests conducted as part of its validation program. More specifically, results from controlled blasting experiments conducted at the Spokane NIOSH research laboratory [5] are used to evaluate the code’s ability to model the extent of damage from a fully coupled explosive charge.

2. Breakage and damage mechanisms in rock blasting

During the detonation of a cylindrical charge, the rock mass within the blast volume experiences direct pressure generated by the initial shock front and subsequently by the influx of explosive gases. During this process both “crushed” and “fractured” zones are generated. In terms of damage adjacent to the blast volume, the practical interest is in determining the extent of the “fractured or disturbed” zones, which in this paper is referred to as the ‘zone of damage’. This zone is mainly formed by a network of minor and major radial cracks, circumferential cracks, and non-radially oriented fractures. Secondary tangential and tensile fractures may develop in this zone from the reflection of stress waves reaching free surfaces [6], [7].

There is some debate as to the dominant mechanisms that contribute to the development of the zone of damage. One school proposes that the main network of fractures is generated by the propagation and interaction of stress waves, while others argue that gas dynamics plays a

much more significant role in both the generation and propagation of fractures. A combination of mechanisms is perhaps the more likely scenario. Mosinets [8] argued that fracturing due to stress waves is the more dominant, contributing approximately 75–88% of the total volume broken with a contribution of only 12–25% by the action of gaseous explosion products. This hypothesis is also supported by the results of full-scale partitioning experiments with blasthole liners reported by Brinkmann [9] and tests conducted by Olsson et al. [10] with the use of emulsions. The importance of gas pressurisation in the propagation of fractures was demonstrated in laboratory scale conditions with synthetic materials by Kutter and Fairhurst [11], Dally et al. [12], and McHugh [13]. There was however little evidence that gas pressurisation was the primary generator of fractures.

Literature suggests that it is almost impossible with current methods to quantify or independently separate the effects of shock and gas in full-scale conditions. This is mainly due to the many complex factors under consideration. They include the dynamics of explosive gas flow, attenuation mechanisms due to leakage into permeable fracture walls, frictional effects, and problems associated with interpreting gas pressure data in structured rock masses [14]. In spite of recent advances in monitoring techniques and instrumentation, the direct application of damage models based on gas pressurisation and fracture mechanics principles such as those proposed by Nilson et al. [15] have not been further pursued. In contrast, the development of models that consider the propagation and interaction of stress waves to infer and/or estimate the extent of fracturing and its relationship to rock breakage and fragmentation is more widespread. A better understanding of the mechanisms involving stress-induced fracturing is evident from the detailed work carried out by investigators such as Starfield and Pugliese [16], Winzer and Ritter [17], Persson et al. [6], Blair and Minchinton [18], Donzé et al. [19] and Rossmanith et al. [20].

As will be described later, the HSBM modelling framework was developed with the view to directly support a combined theory of damage and overall fragmentation that is, a theory where the intensity, propagation, and interaction of stress waves are the dominant fracturing mechanisms (i.e., conditioning stage), with gas flow influencing the later stages of breakage and displacement of fragments.

3. Modelling dynamic fracturing, fragment formation, and displacement in rock blasting

It is beyond the scope of this paper to review in detail all of the modelling techniques published to date; however, some notable examples are reported to illustrate the capabilities and limitations of different approaches. This review also puts into context the main reason why an improved numerical technique was developed and implemented as part of the HSBM project.

Several attempts have been made to simulate the dynamic fracturing process, fragment formation, and displacement in blasting. The numerical methods used are based on finite element, finite difference, and discrete element. They have been applied in isolation and in combined forms. In most cases, shock wave propagation and the fracturing process have been modelled with finite element and finite difference codes. Discrete element codes have

mainly been applied to model particle motion or rock movement problems. In all three types of numerical techniques, the geometry of the rock mass is divided into a number of small elements or zones which is referred to as “discretisation”. The behaviour of each element/zone in the model is governed by a “constitutive law”. If the constitutive law is appropriate and all of the relevant mechanisms are represented, the model is expected to behave as the material being represented. The difference between all three numerical approaches is in the treatment of the elements and how the behaviour of each is “summed” to represent the problem as a whole.

In the case, for example, of a hydrodynamic finite element code such as LS-DYNA2D and LS-DYNA3D, commercially developed by Livermore Software Technology Corporation [21], damage and fragmentation is predicted by the introduction of constitutive laws such as the Taylor–Chen damage model [22]. Such constitutive laws are required in numerical models to relate the magnitude of stress at a point in the rock-to-rock failure. The Taylor–Chen model has a rate-dependent brittle failure criterion that is based on the growth and interaction of pre-existing micro-cracks in the material.

Sophisticated finite element/discrete element hybrid codes such as ELFEN, commercially developed and marketed by Rock-field Software Ltd, can perform both two-dimensional and three-dimensional analysis of stress, fracturing, and in-flight block interaction of the blasting process. The code’s capabilities were improved with the integration of the MBM2D model developed by Munjiza and Owen [23], Owen et al. [24], and Minchinton and Lynch [25]. In MBM2D the detonation process is modelled using a non-ideal detonation code called CPeX [26], which provides the velocity of detonation and the borehole pressure history as input [25].

The geometry of an ELFEN model is discretised into distinct polygonal elements that are divided into finite elements. This is equivalent to the schemes adopted by other discrete element codes such as UDEC and 3DEC of the Itasca group. The most significant difference between ELFEN and the two Itasca codes is that the former has a fracturing scheme that causes a finite element to “break” according to a fracture-based, Rankine plasticity model [25]. The fracturing of an element occurs when either the tensile strength of the rock has been reached or if the stresses in the element are zero as a result of the post-peak softening rule. Dare-Bryan et al. [27] have reported that ELFEN does not incorporate a gas flow code to model the expansion of gases through the fractures, and that it is difficult and computational intensive to incorporate discontinuities.

A discrete element code that has been used to model the combined mechanical effect of stress waves and high pressure gas flow is the particle flow code PFC3D developed by Itasca Inc [28]. In this technique, a model is composed of distinct particles that displace independently from one another and interact only at contacts. PFC3D allows finite displacements and rotations of discrete bodies (including complete detachments) and recognizes new contacts automatically as the calculation progresses. It is important to note that the original computational kernel of the HSBM model was based on the implementation of PFC3D [29]. As will be explained later, this has been superseded by a continuum and discontinuum hybrid approach that combines the explicit finite difference code FLAC and a

newly developed lattice scheme [30], [31]. This new implementation was driven by the difficulty and computational effort required to model a complete blasting configuration with PFC3D. It is interesting to note that successful attempts using a simpler implementation of discrete element codes to simulate dynamic fracture formation have been documented elsewhere [19]. Results from these attempts support the view that particle flow codes could be successfully implemented in an advanced blasting model.

In general, the success of earlier models indicated that an improved code that could simulate detonation, rock fracture and displacement must incorporate fundamental principles of detonation theory (ideal and non-ideal), stress wave propagation and interaction in a jointed rock mass, gas flow, the ability to model continuum and discontinuum behaviour; and the ability to explicitly consider the effect of different boundary conditions. This has been achieved within the HSBM framework and the final validation and commissioning of the model is currently being conducted. This paper discusses one particular case study that contributes towards the validation of this new numerical modelling approach.

4. The Hybrid Stress Blasting Model (HSBM)

The Hybrid Stress Blasting Model (HSBM) can be described as a sophisticated blast modelling research tool. The code has been under development for the last 10 years through an international collaborative research project funded by a consortium of companies acknowledged in this paper, comprising explosive and equipment suppliers and major mining houses. Over the course of its development, several improvements and modifications have been made to both the detonation and geomechanical modelling components in order to improve calculation speed and the size of problem that could be modelled.

A description of the original HSBM framework has been given in [29], and has been updated in [30,31]. The main components and software links that have not changed since the inception of the project include:

4.1. Detonation modelling

Ideal and non-ideal detonation models are used to model explosive detonation characteristics for fully coupled and decoupled conditions. The current detonation module in HSBM is designated as Vixen. It is envisaged that this may be replaced by a Direct Numerical Solution (DNS) approach to more accurately account for blast confinement effects.

4.2. Blast layout and discrete fracture network (DFN)

These include blast layout and discontinuity software tools that enable the design of larger and more complex models and blasting layouts. However, the rock-breakage engine has the ability to build relatively simple blast geometries based on built-in design templates.

4.3. The rock breakage engine

The rock breakage engine in the HSBM is designated Blo-Up. It uses a combination of continuous and discontinuous numerical techniques to model detonation, dynamic wave propagation, rock fragmentation, and muck pile formation.

The Blo-Up interface is a platform for model-entering input parameters as well as a graphical display of specific outputs. These include 3D graphical representations of dynamic fracturing, fragment size distributions, internal fragment damage, pressure histories, and velocity histories. Confidentiality agreements currently preclude publication of detailed information on all algorithms. The mechanical aspects of the Blo-Up computational engine have been discussed in detail in [30]. One of the most fundamental aspects of the code is the numerical representation of the borehole, explosive charge, and rock mass.

As described by Furtney et al. [30], the borehole explosive and near field rock are represented as an axis-symmetric continuum using the FLAC code [32]. The explosive is represented as a special constitutive behaviour in the central zones of the FLAC region. The detonation models (described separately in [33]), determine the velocity of detonation (VoD), parameters for the Williamsburg equation of state, the final reaction extent, the initial density, and a reference state. Energy release in the FLAC zones representing the explosive is controlled by a programmed burn (PB) algorithm [34]. As shown in Fig. 1, the rock in the near field area is represented as a Mohr–Coulomb material, which is coupled to the explosive reaction products represented by the Williamsburg model. Energy released by the reaction increases the isotropic stress in the zones representing the explosive. The confining material expands in response to the increasing gas pressure, and the new confining volume is transmitted to the Williamsburg equation of state, which returns a new isotropic stress. In this way, rock and explosive are fully coupled at all times. The stemming material is modelled directly as a Mohr–Coulomb material. The mechanical calculation is fully coupled to a simplified gas flow logic representing the high-pressure reaction product gas. This logic uses an equilibrium pressure multiplier to simulate energy losses due to crushing of the borehole wall.

The rock mass is represented with a lattice-type discrete element method which is a simplification of the full DEM calculation cycle previously performed by the PFC3D code. The main features of the lattice approach have been described by Cundall [35] where, in general terms, the lattice method applies forces to point masses which only have translational degrees of freedom, and the connecting springs have a tensile breaking strength. This simplification has resulted in an increase in calculation speed and a significant decrease in memory storage requirements. The model geometry is built up of point masses distributed in a non-repeating pattern with a user-specified average separation between nodes (i.e., model resolution). Fig. 1 shows a schematic of the lattice. Lattice nodes that overlap FLAC zones are velocity-controlled by the movement in the FLAC zones. The lattice nodes then contribute a force back to the FLAC zones. This mechanism provides direct coupling between the lattice region and the borehole representation.

The equation of motion for a point mass (node) in the lattice is

$$\sum \vec{f} = m(\ddot{\mathbf{x}} - \vec{g}) \quad (1)$$

where $\Sigma \vec{f}$ is the sum of the unbalanced forces acting on a node, m is the node mass, $\vec{g}$ is the acceleration due to gravity and **x** is the node position in 3D space. The dots over **x** imply derivatives with respect to time.

$$\sum \overrightarrow{f} = \overrightarrow{f}\, c + \overrightarrow{f}\, d \quad (2)$$

In Eq. (2) the sum of forces is composed of the force from lattice springs, $\vec{f}c$, and a viscous damping force, $\vec{f}d$. The force from the lattice springs is proportional to the distance between the nodes, This can be written incrementally as

$$\Delta\, \overrightarrow{f}\, c = kn \left(\dot{\mathbf{x}}^{n1} - \dot{\mathbf{x}}^{n2} \right) \Delta t \quad (3)$$

where kn is the normal contact stiffness and Δt is the integration time step. This assumes that the normal stiffness and shear contact stiffness are the same. Material properties are discussed in the next section. The normal contact stiffness kn is taken as the average of the nodes attached to a spring as

$$kn = \frac{kn^{n1} + kn^{n2}}{2} \quad (4)$$

The force in the direction of a given spring is

$$\overrightarrow{f}\, ns = \left| \mathbf{x}^{n1} - \mathbf{x}^{n2} \right| \times \overrightarrow{f}\, c \quad (5)$$

Each spring has a tensile strength, which is the average of the tensile strengths of the attached nodes. If the force on a given spring $\vec{f}_{ns}$ exceeds this tensile strength, the spring breaks and is removed from the lattice. Removing springs from the lattice removes the strain energy the spring contained. Viscous damping is added to the lattice springs to account for the attenuation observed in real rock. The spring damping force is defined as

$$\overrightarrow{f}\, d = \eta\alpha \left(\dot{\mathbf{x}}^{n1} - \dot{\mathbf{x}}^{n2} \right) \quad (6)$$

$$\text{where} \quad \eta = \sqrt{m k_n} \quad (7)$$

and α is a damping coefficient that may be set from zero to unity. A value of zero corresponds to no-damping; a value of unity corresponds to critical damping. A leap-frog integration scheme is used to solve the equation of motion for individual nodes. Using the central-difference approximation, the acceleration of a node can be written as

$$\ddot{\mathbf{x}}^t = \frac{1}{\Delta t}\left(\dot{\mathbf{x}}^{t+\Delta t/2} - \dot{\mathbf{x}}^{t-\Delta t/2}\right) \quad (8)$$

where $\dot{\mathbf{x}}^{t+\Delta t/2}$ is the node velocity a half-time step in the future and $\dot{\mathbf{x}}^{t-\Delta t/2}$ is the node velocity a half-time step in the past. Substituting this form into Eq. (1) gives

$$\dot{\mathbf{x}}^{t+\Delta t/2} = \dot{\mathbf{x}}^{t-\Delta t/2} + \left(\frac{\sum \vec{f}^t}{m} + \vec{g}\right) \quad (9)$$

The node position **x** is updated by

$$\mathbf{x}^{t+\Delta t} = \mathbf{x}^t + \left(\dot{\mathbf{x}}^{t+\Delta t/2}\right)\Delta t \quad (10)$$

In this numerical representation, standard material properties can be specified by the user. These include Young's modulus (E), Poisson's ratio (ν), density (ρ), unconfined compressive strength (UCS), direct tensile strength (T), friction angle (ϕ), and a damping coefficient (α). The parameters for the Mohr–Coulomb constitutive model are all derived from the above properties. The lattice normal-contact stiffness and spring tensile strength are dependent of the lattice resolution and are defined by

$$k_n = lC_k K \quad (11)$$

$$t_s = l^2 C_t T \quad (12)$$

where l is the lattice resolution, C_k and C_t are calibration parameters with values near unity, K is the bulk modulus, t_s is the spring tensile strength, and T is the direct tensile strength.

Four boundary conditions are permitted on the lattice—free, quiet, semi-quiet, and flex. Free nodes represent a free surface, which may reflect stress waves. Quiet boundaries are used to model intact rock of the same type in the far field. Quiet boundaries ensure that wave energy is absorbed at the interior (artificial) model boundaries. Semi-quiet boundaries represent impedance boundaries in the far field at which some wave energy is returned into the rock body. The flex-boundary condition is used to represent boundaries between the intact rock mass and compactable broken rock.

5. Controlled blasting experiments

Data from controlled blasting experiments in large concrete blocks was made available to the HSBM group by a research team at the Spokane Office of Mine Safety and Health Research (OMSHR), part of the National Institute for Occupational Safety and Health (NIOSH) in the U.S.A. The principal aim of the experimental work was to investigate the damage zone resulting from fully coupled charges using conventional mining explosives. These experiments form part of a wider research program at NIOSH that aims at minimising

the amount of unwanted damage to the perimeter of underground excavations. Details of the experimental program have been documented in detail in [5].

The experimental work consisted of two stages. The first involved testing a fully instrumented concrete block 3.0 m wide by 3.0 m long and 1.5 m high. This preliminary test is described in this section and the results used to evaluate and calibrate the lattice scheme in the HSBM model. In the second stage, a block 3.7 m wide by 2.4 m long and 1.8 m high was tested. The calibrated HSBM model was used to predict *a priori* the extent of damage from this modified geometry test. Predictions were compared to directly mapped fractures in the test.

5.1. Stage 1 experimental setup and test results

The stage 1 concrete block test is shown in Fig. 2. A 38-mm-diameter blasthole was percussion-drilled to a length of 1.8 m. It was collared 813 mm from the bottom of the block, with a burden of 45 cm and charged with a packaged emulsion product that was gently loaded and tamped into the hole to achieve full coupling (i.e., Dyno® AP, Dyno Nobel). The fully coupled charge was approximately 1.2 m in length. The basic properties of the explosive charge included a density of 1.15 g/cm^3, an unconfined velocity of detonation of 4700 m/s, and a heat of reaction of 3.24 MJ/kg.

The physical properties of the concrete block available at the time the HSBM model was evaluated are summarised in Table 1 below.

As shown in Fig. 2, the block was instrumented with an array of strain gauge sensors, accelerometers and geophones. The aim of the instrumentation setup was to study the relationship between explosive induced stresses and the final extent of damage. Details of the stage 1 test results are well documented in [5]. Surface damage patterns were quantified using a laser scanner after loosened material was removed. Fig. 3 shows the post blast block along with one laser profile section showing the extent of damage after two layers of scaling. A 76-mm-diameter inspection hole was diamond drilled normal to the blasthole axis and a borehole camera was used for visual inspections. A radial crack was identified approximately 60 cm away from the blast-hole position. This crack was confirmed in the Micro-Velocity Probe (MVP) data collected and documented in [5]. Three wire saw cuts were made normal to the blasthole at distances of 0.69 m, 1.22 m, and 1.60 m from the blasthole collar. Radial cracks were easily identified on the wire saw cut surfaces. The cracks were highlighted with a permanent marker, laser scanned, digitized, and exported as a profile into AutoCAD. The crack profile from the first cut at 0.69 m measured from the blasthole collar is shown in Fig. 4. This cut aligns closely with the embedded strain gauge array. Results show major radial cracks up to a limit of approximately 1.76 m.

Ultrasonic measurements were also conducted on the NX core using a cross-core P-wave measurement device. The core was placed in a special holder and the transmitter and receiver transducers oriented across the diameter. As reported by Iverson et al. [5], the time required for a P-wave to traverse the diameter was recorded. From the data, a plot of sonic velocity as a function of distance from the blasthole was constructed. From this analysis a damage limit of approximately 0.5 m was identified at 95% of the measured background

velocity. Brazilian tests were also performed on sections of the core extracted from the inspection hole at defined distances from the blasthole. Analysis of strength versus distance also indicated a damage limit approximately 0.5 m at 95% of the measured background strength.

Fig. 5 shows the recorded peak radial strain for the strain gauge closest to the blasthole (e.g., 0.23 m). The peak strain in the radial direction translated to a peak particle velocity of approximately 18.1 m/s.

6. Evaluation and calibration of the HSBM

As discussed earlier, the stage 1 experimental results were used to make preliminary evaluations of the code using solution parameters based on smaller laboratory scale tests in concrete available to the authors. The model geometry and velocity history locations are described in Fig. 6. The lattice resolution in this model was 38 mm, the damping coefficient was 0.1, the equilibrium pressure multiplier was 0.5 and the strength attenuation parameters were M=10 and b= −1.5. The equilibrium pressure multiplier describes the energy losses during the borehole crushing stages. The strength attenuation parameters are included in the HSBM framework to emulate the complex dependency between strain rate and strength. The lattice method applies forces to point masses, which have only translational degrees of freedom, and the connecting springs have a tensile breaking strength. The known dependency of tensile strength on strain rate has been implemented with a simple model where the tensile strength is scaled by a power law function of distance away from the nearest borehole:

$$T=\frac{(M-1)}{{r_0}^{-b}}r^b+1 \quad (13)$$

where T is the tensile strength multiplier, r_0 is the radius of the borehole, r is the length from the nearest hole, M and b are parameters which allow to scale the dynamic tensile strength.

The charge length was 1.2 m for an emulsion product at a density of 1.15 g/cm^3. In this particular case, data from the strain gauge nearest to the blasthole was used to calibrate the near field response of the model. During the calibration phase, a simple iterative process was adopted to gain a good understanding of the sensitivity of final results to specific changes in model solution parameters. The objective of the evaluation stage was to achieve a close match between direct measurements from the stage 1 test and modelling results. It should be noted that the physical properties of the concrete block available at the time of this study were not modified in any way and were equivalent to those described in Table 1.

Fig. 7 shows plan view sections sliced along the centre of the borehole displaying velocity fields describing propagation of the primary stress wave initiated by detonation of the explosive charge. The development of the Mach cone from the initiation point (toe of blasthole) can be observed from these images. A graph of particle velocity versus time next to each frame identifies the arrival of the stress wave at the assigned history points as well as the peak particle velocity experienced in the radial (Y) direction at the nearest and furthest history point in the model. As shown in Fig. 7, the peak particle velocity of approximately

17 m/s closely matches the measured value inferred from the peak strain reported earlier (18.1 m/s).

The resulting fracture patterns, fragment formation and extent of damage after 20 ms are shown in Fig. 8. Several sections are plotted here to describe the overall pattern of fractures and damage near the free face and the bottom boundary. Note that the damage extent depends clearly on the direction of propagation and interaction of the stress wave with respect to the block boundaries. Fig. 8 shows, in black and red dots, the maximum extent of internal damage for a section located at a distance equivalent to the inspection hole drilled in the physical experiment. As shown, the radius of damage is of the order of 0.6 m from the centre of the borehole. This compares well with the 50-cm limit measured in the experiments. It is also important to note that the model appears to overestimate the degree of damage in the far corner of the block. This is attributed to a limitation in the attenuation model adopted in the current lattice scheme, associated with a constant damping coefficient. This is reinforced by the peak particle velocity predicted by the model in the furthest measuring point (i.e., 2 m/s). Strain gauge data at this location indicated a peak value of 700 mm/s.

7. HSBM damage predictions—Validation case

As a validation case, damage predictions were made for a different experimental configuration. Results from the physical experiment were not available to the HSBM project team until predictions were made and reported. The aim was to test the ability of the model to predict, *a priori*, the extent of breakage and damage for a new set of charging parameters in a concrete block with slightly different geometry and mechanical properties. Fig. 9 shows the geometry of this test, referred to as the stage 2 experiment. As before, a 38-mm-diameter blasthole was drilled from the front to the back of the block (i.e., 2.4 m long). The drillhole was collared at block mid-height with a burden of 15.2 cm (0.152 m); and charged with an emulsion product (i.e., Orica Senatel Magnafrac). The basic properties of the explosive charge included a density of 1.11 g/cm^3 and a measured velocity of detonation of 5050 m/s in the 38-mm-diameter blasthole. The physical properties available to the analysis are summarised in Table 2 below. As mentioned earlier, these properties vary slightly from those of the stage 1 concrete block.

Fig. 10 shows the HSBM model configuration. Model solution parameters were similar to the calibration test, with a model resolution of 38 mm, a damping coefficient of 0.1, an equilibrium pressure multiplier of 0.5; and strength attenuation parameters M=10 and b= −1.5. These parameters were kept constant to predict the effect of this new block geometry, explosive charge, and material properties. Charging conditions were similar to the physical test (e.g., emulsion at a density of 1.11 g/cm^3). The physical properties of the concrete block applied to this model were those described in Table 2.

Fig. 11 shows modelling results after 20 ms. At this time, the burden volume was fragmented and ejected. Major fractures (in black) and internal damage (in red) are also plotted in this image. The images describe the complex shape of the damage zone associated with the influence of point of initiation and boundary conditions. As shown on the plan view

section, the extension of damage is greater near the hole collar than at the toe (point of initiation) of the explosive charge. Fig. 12 shows a direct comparison between model predictions and actual results from this test configuration. The slice is taken at the centre of the explosive charge. The shape and extent of fracturing predicted by the model closely matches actual measurements. Radial fractures extending towards free faces are apparent in the modelling output and match those mapped after the physical experiment. As shown in the superimposed images in Fig. 12, the maximum extent of visible damage was on the order of 1.45 m.

Fig. 13 shows both predicted and measured particle velocities in the near field, indicating a relative difference of only 1.59% at the nearest history point (i.e., 0.3 from the explosive charge). Discrepancies become larger further away from the charge with relative differences of −22.4% and −42.9% at distances of 0.46 m and 0.61 m, respectively. This shows that the model appears to overestimate peak radial velocities. As discussed in the calibration stage, this deficiency was expected. The lack of attenuation produces an overestimation of the expected damage at the corner of the block in question (also highlighted in Figs. 11 and 12). However, the extent of visible damage in the near field adequately matches direct measurements. The model has the added advantage of highlighting areas of potential internal (invisible) damage.

8. Conclusions and future work

The Hybrid Stress Blasting Model (HSBM) can be described as a sophisticated blast modelling research tool. The code has been under development for the last 10 years through an international collaborative research project funded by a consortium of companies acknowledged in this paper and comprising explosive and equipment suppliers and major mining houses. Over the course of HSBM development, several improvements and modifications have been made to both the detonation and geomechanical modelling components. These improvements have increased calculation speed and problem size. This paper describes the results from controlled blasting experiments conducted at the Spokane NIOSH research laboratory, and evaluates the code’s ability to predict the extent of damage from a fully coupled explosive charge. Conclusions of this work can be summarised as follows:

The code is capable of adequately predicting both the extent and shape of the damage zone including the influence of point of initiation and free face boundary conditions. Radial fractures extending towards free faces are apparent in the modelling output and match those mapped in the physical experiment. The maximum extent of visible damage was of the order of 1.45 m.

The code predicted peak radial velocities within a relative difference of only 1.59% at the nearest history point (0.3 m from the explosive charge) with discrepancies becoming larger further away from the charge. Relative differences of −22.4% and −42.9% occurred at distances of 0.46 m and 0.61 m, respectively, meaning that the model overestimated particle velocities at these distances. The deficiency in the modelling of attenuation produced an

overestimation of the expected damage zone at the corner of the modelled block because modelled stress reflections were excessive.

Ongoing work includes further developments of the near field and gas logic and additional sensitivity analysis to better understand the influence of model solution parameters on attenuation. Longer term, a full validation program is planned to support full-scale applications.

Acknowledgments

The authors would like to thank the sponsors of the HSBM project who are currently African Explosives Limited Mining Services, Limited, De Beers, Anglo American, Codelco Chile, LKAB, Sandvik Mining and Construction, Dyno Nobel Asia Pacific and Rio Tinto. The authors would also like to thank Peter Cundall for all of his contributions.

References

1. Cundall P, Hart R. Numerical modelling of discontinua. Eng Comput. 1992; 9:101–13.
2. Bobet A, Fakhimi A, Johnson S, Morris J, Tonon F, Ronald Yeung M. Numerical models in discontinuous media: review of advances for rock mechanics applications. J Geotech Geoenviron Eng. 2009; 135:1547–61.
3. Munjiza A. Special issue on the discrete element method: aspects of recent developments in computational mechanics of discontinua. Eng Comput. 2009; 26:1.
4. Guest, AR. The dynamic breakage of Kimberlite in the near field. Brisbane, Australia: University of Queensland; 2004.
5. Iverson, SR.; Hustrulid, WA.; Johnson, JC.; Tesarik, D.; Akbarzadeh, Y. Proceedings of the ninth international symposium on rock fragmentation by blasting. Granada, Spain: Taylor & Francis; 2009. The extent of blast damage from a fully coupled explosive charge; p. 459-68.
6. Persson, PA.; Holmberg, R.; Lee, J. Rock blasting and explosives engineering. Boca Raton: CRC Press; 1994.
7. Song, J.; Kim, K. Blasting induced fracturing and stress field evolution at fracture tips. Proceedings of the 35th US rock mechanics symposium; Reno, Nevada. 1995; p. 547-52.
8. Mosinets V. Mechanism of rock breaking by blasting in relation to its fracturing and elastic constants. Sov Min Sci. 1966; 2:492–9.
9. Brinkmann, JR. An experimental study of the effects of shock and gas penetration in blasting. Proceedings of the third international symposium on rock fragmentation by blasting; Brisbane. 1990; p. 55-66.
10. Olsson, M.; Nie, S.; Bergqvist, I.; Ouchterlony, F. What causes cracks in rock blasting?. Proceedings of EXPLO ‘01 conference; Hunter Valley, Australia: Australasian Institute of Mining and Metallurgy; 2001. p. 319-29.
11. Kutter HK, Fairhurst C. On the fracture process in blasting. Int J Rock Mech Min Sci. 1971; 8:181–8.
12. Dally JW, Fourney WL, Holloway DC. Influence of containment of the bore hole pressures on explosive induced fracture. Int J Rock Mech Min Sci. 1975; 12:5–12.
13. McHugh S. Crack extension caused by internal gas pressure compared with extension caused by tensile stresses. Int J Fract. 1983; 21:163–76.
14. Lymbery, SC. PhD thesis. University of Queensland; 2001. Hydrodynamic extension of radial fractures by explosive gas loading.
15. Nilson RH, Proffer WJ, Duff RE. Modelling of gas driven fractures induced by propellant combustion within a borehole. Int J Rock Mech Min Sci. 1985; 22:3–19.
16. Starfield AM, Pugliese JM. Compression waves generated in rock by cylindrical explosive charges: a comparison between computer and field measurements. Int J Rock Mech Min Sci. 1968; 5:65–77.

17. Winzer SR, Ritter AP. Role of stress waves and discontinuities in rock fragmentation. Int J Blast Fragment. 1985:11–23.
18. Blair D, Minchinton A. On the damage zone surrounding a single blasthole. Int J Blast Fragment. 1997; 2:59–72.
19. Donzé FV, Bouchez J, Magnier SA. Modeling fractures in rock blasting. Int J Rock Mech Min Sci. 1997; 34:1153–63.
20. Rossmanith H, Daehnke A, Knasmillner R, Kouzniak M, Ohtsu M, Uenishi K. Fracture mechanics applications to drilling and blasting. Fatig Fract Eng Mater Struct. 1997; 20:1617–36.
21. LSTC. Livermore Software Technology Core Home Page. Oct 2. 2001 <http://www.dyna3d.com/>
22. Taylor LM, Chen PE, Kuszmaul JS. Microcrack-induced damage accumulation in brittle rock under dynamic loading. Comput Meth Appl Mech Eng. 1986:301–20.
23. Munjiza A, Owen RJ. Discrete element models of rock blasting. Eng Model. 1992; 5:65–73.
24. Owen, DRJ.; Munjiza, A.; Bicanic, N. A finite element–dicrete element approach to the simulation of rock blasting problems. Proceedings eleventh symposium on finite element methods; Cape Town. 1992; p. 39-58.
25. Minchinton, A.; Lynch, PM. Fragmentation and heave modelling using a coupled discrete element gas flow code. Proceedings of the fifth international symposium on rock fragmentation by blasting; Montreal. Rotterdam: Balkema; 1996. p. 71-80.
26. Kirby, IJ.; Leiper, GA. A small divergent detonation theory for intermolecular explosives. Proceedings of the eighth international symposium on detonation; Office of Naval Research; 1985.
27. Dare-Bryan, P.; Wade, L.; Randall, M. Computer modelling of bench blasting for grade control. Proceedings of the 27th international symposium on rock fragmentation by blasting; Orlando, Florida: International Society of Explosive Engineers; 2001. p. 13-24.
28. Potyondy, DO.; Cundall, PA.; Sarracino, RS. Modelling of shock and gas-driven fractures induced by a blast using bonded assemblies of spherical particles. Proceedings of the fifth international symposium on rock fragmentation by blasting; Montreal, Canada. Rotterdam: Balkema; 1996. p. 55-62.
29. Ruest, M.; Cundall, P.; Guest, A.; Chitombo, G. Developments using the particle flow code to simulate rock ragmentation by condensed phase explosives. Proceedings of the eighth international symposia on rock fragmentation by blasting; Santiago, Chile. Editec. 2006; p. 140-151.
30. Furtney, JK.; Cundall, PA.; Chitombo, GP. Developments in numerical modeling of blast induced rock fragmentation: updates from the HSBM project. Proceedings of the ninth international symposium on rock fragmentation by blasting; Granada, Spain. London: Taylor & Francis; 2009. p. 335-342.
31. Furtney, JK.; Cundall, PA.; Onederra, I.; Sellers, E. continuum and distinct element numerical modeling in geomechanics-2011. Melbourne. Minneapolis: Itasca; 2011. Numerical modeling of rock blasting: Validation tests for Blo-Up 2.5; p. 2-9.
32. Group I.C.F.L.A.C. (Fast Lagrangian Analysis of Continua), Version 6.0. Minneapolis: Itasca; 2008.
33. Braithwaite, M.; Sharpe, G.; Chitombo, G. Simulation of real detonations as an energy source term for the Hybrid Stress Blasting Model. In: Sanchidrián, JA., editor. Ninth international symposium on rock fragmentation by blasting. Spain: Granada; 2009. p. 327-33.
34. Kapila AK, Bdzil JB, Stewart BS. On the structure and accuracy of programmed burn. Combust Theor Model. 2006; 10:289–321.
35. Cundall, P. Lattice method for modeling brittle, jointed rock. Melbourne. Minneapolis: Itasca; 2011. Continuum and distinct element numerical modeling in geomechanics—2011; p. 1-9.

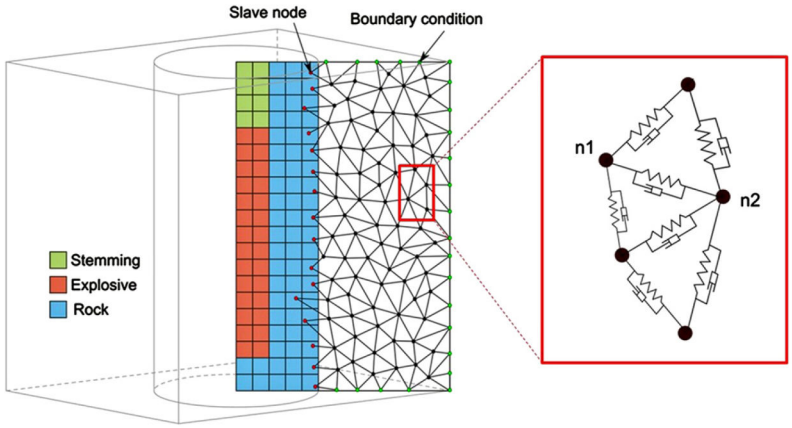

Fig. 1.

Schematic representation of the FLAC zones and lattice nodes are connected together with springs and dashpot elements in parallel (after [30]).

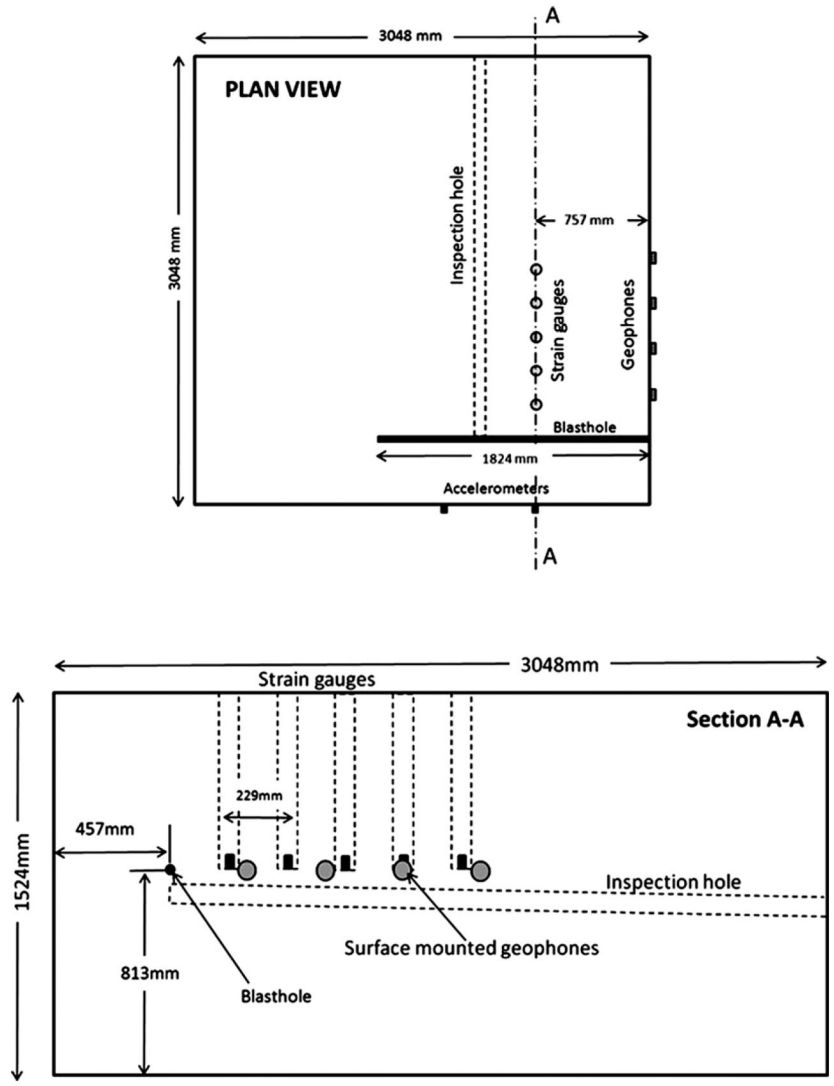

Fig. 2.
Stage 1 concrete block geometry and experimental setup (after [5]).

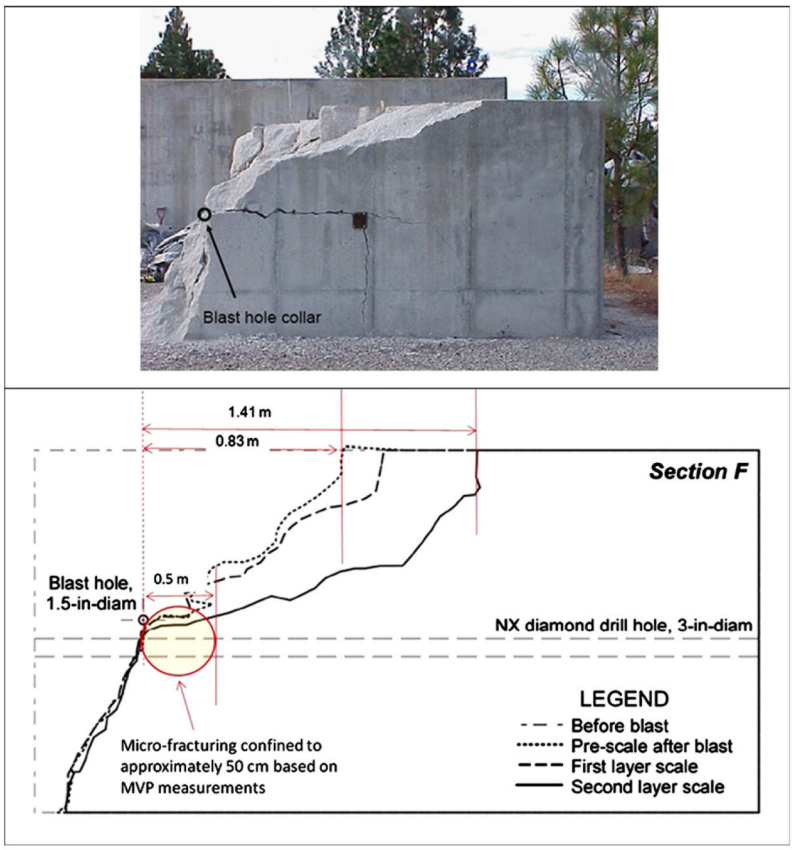

Fig. 3.
Example of post blast results of the stage 1 concrete block test (after [5]).

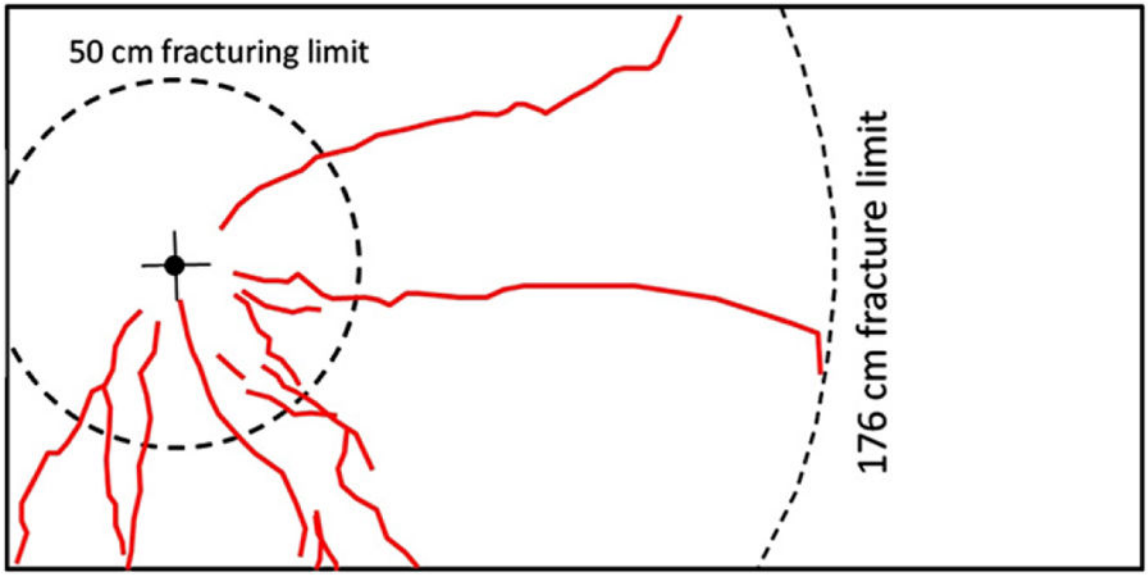

Fig. 4.
Example of digitised radial fracture patterns from wire saw cutting section (after [5]).

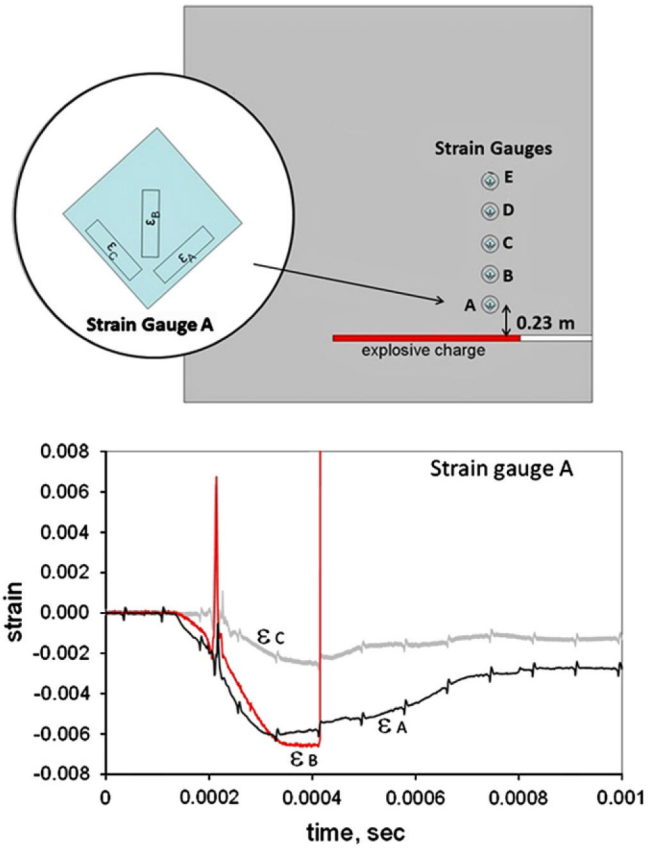

Fig. 5.
Peak strain measured 0.23 m away from the explosive charge (after [5]).

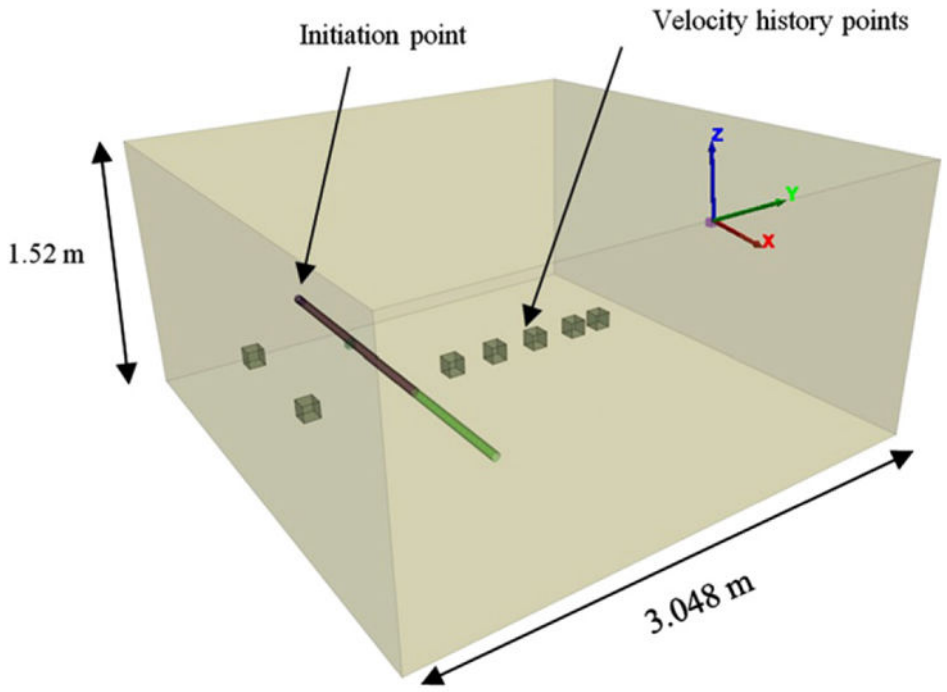

Fig. 6.
HSBM model configuration of the stage 1 concrete test.

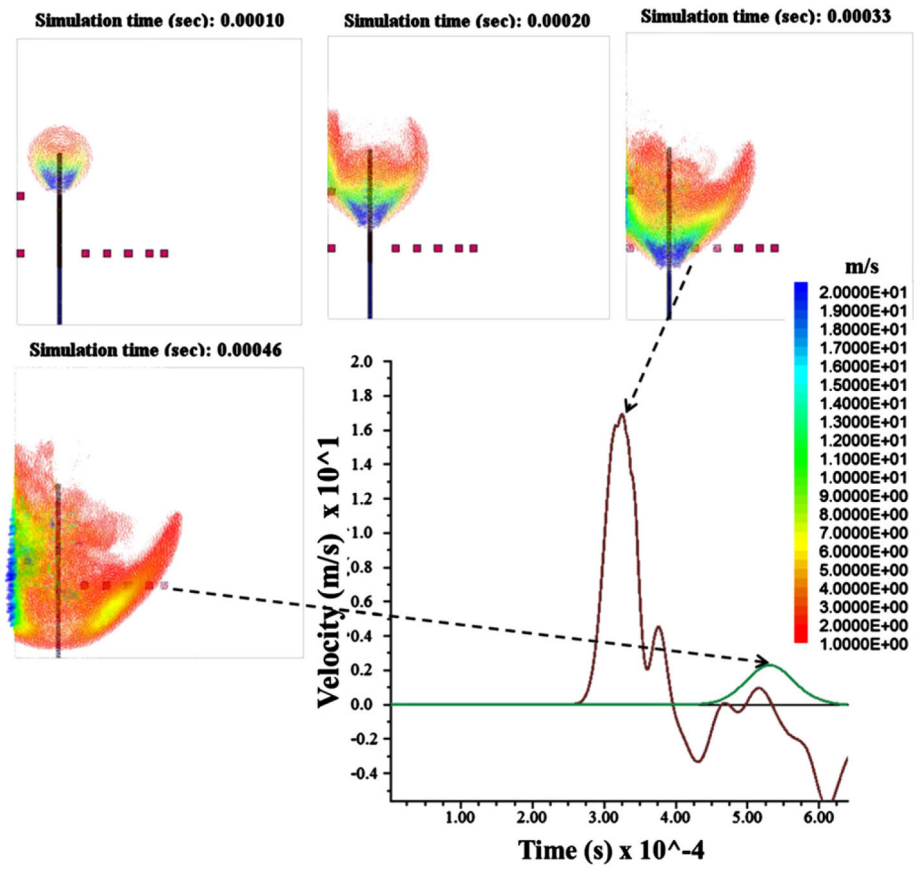

Fig. 7.

Plan view of slices along the blasthole charge showing contours of velocity fields representing the propagation of the primary stress wave together with peak radial velocity of two strain gauge positions.

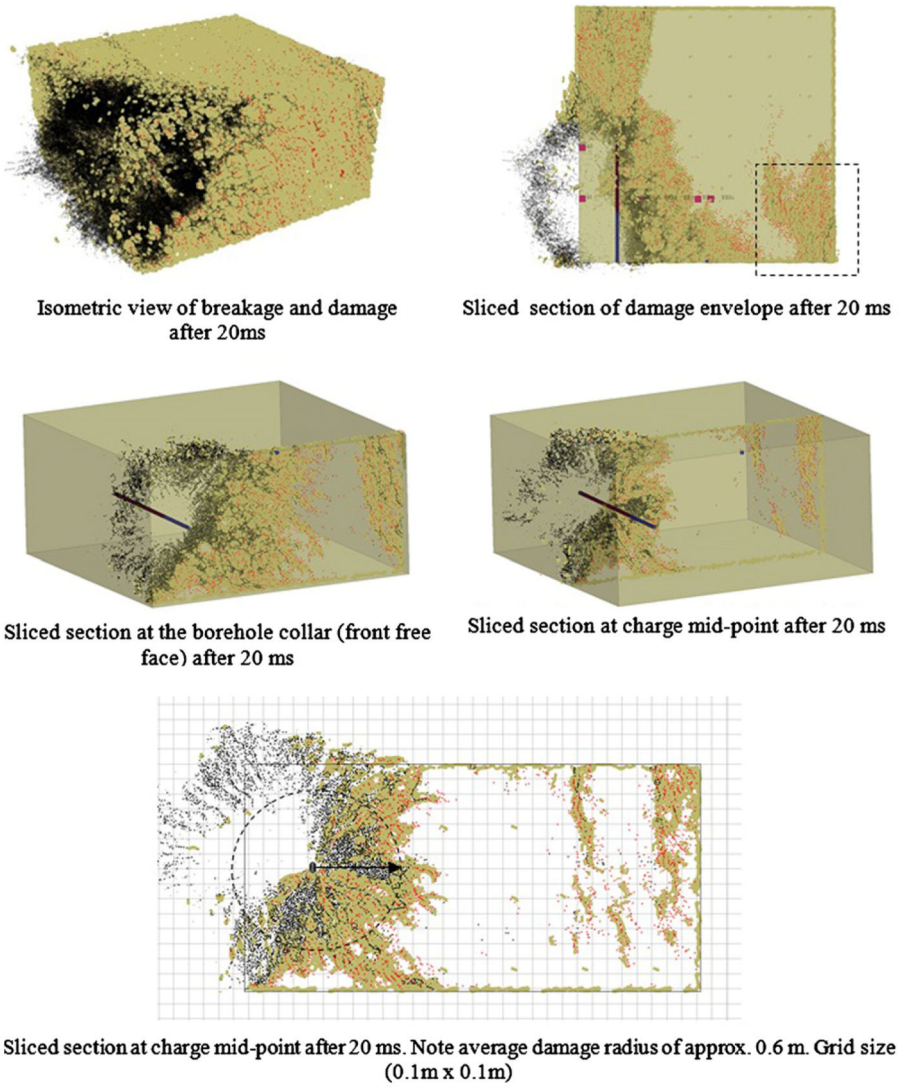

Fig. 8.

Modelling results of the extent of damage for the stage 1 calibration block.

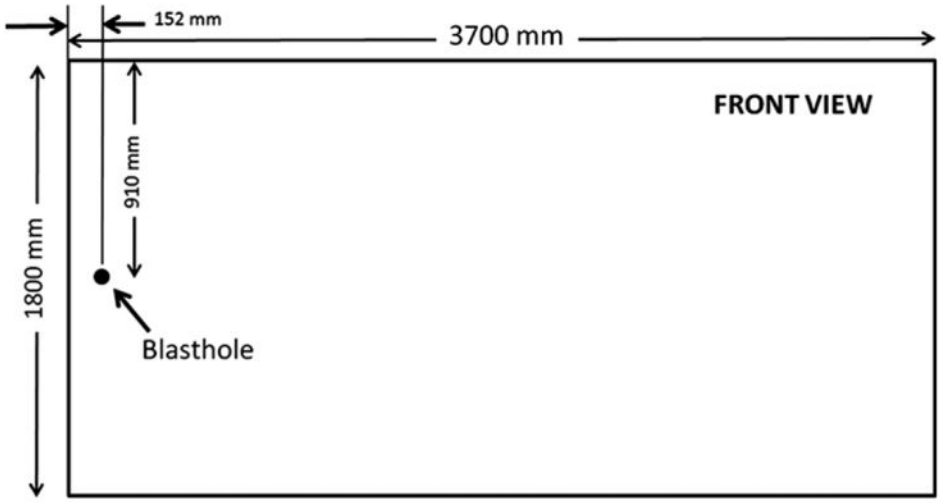

Fig. 9.
Stage 2 concrete block geometry and experimental setup.

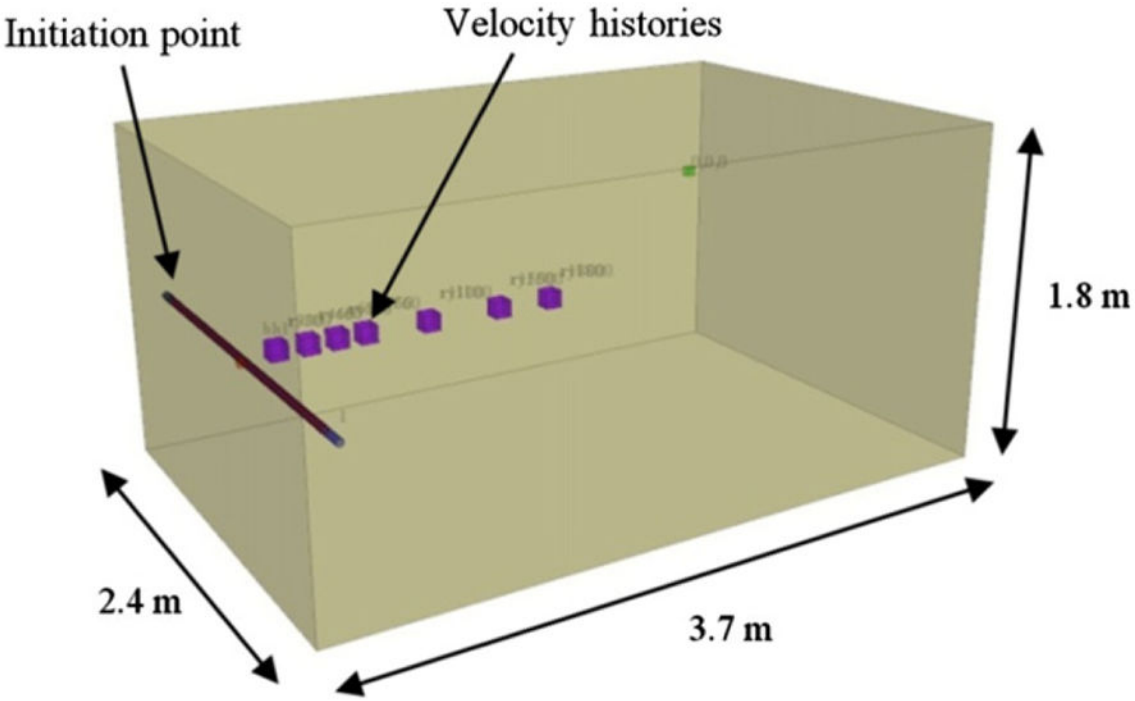

Fig. 10.
HSBM model configuration and input parameters for the stage 2 concrete block experiment.

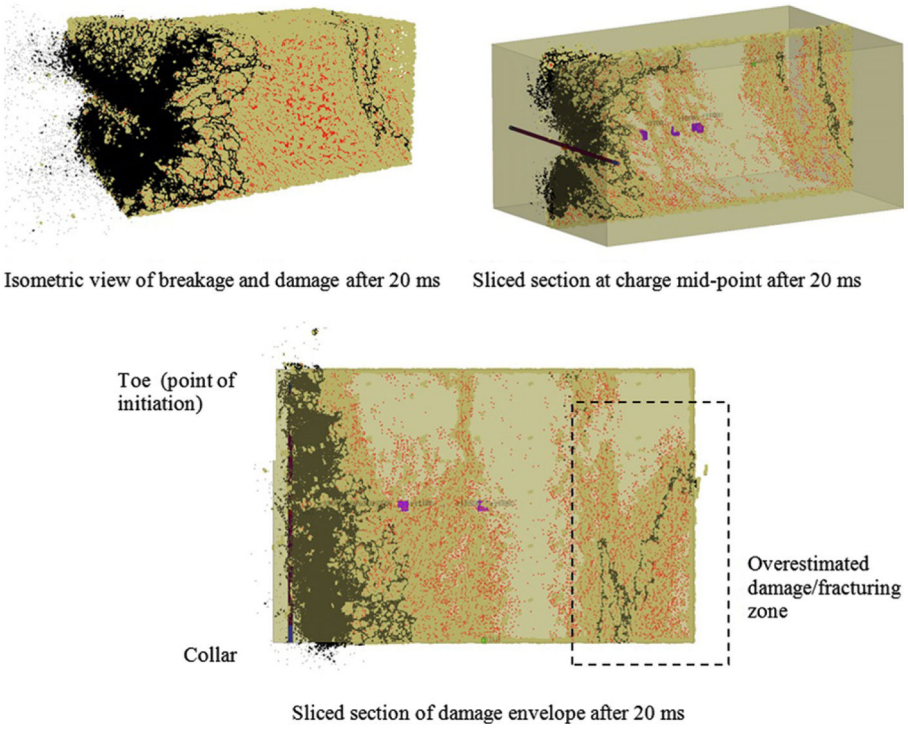

Fig. 11.
HSBM modelling predictions of the stage 2 concrete block experiment.

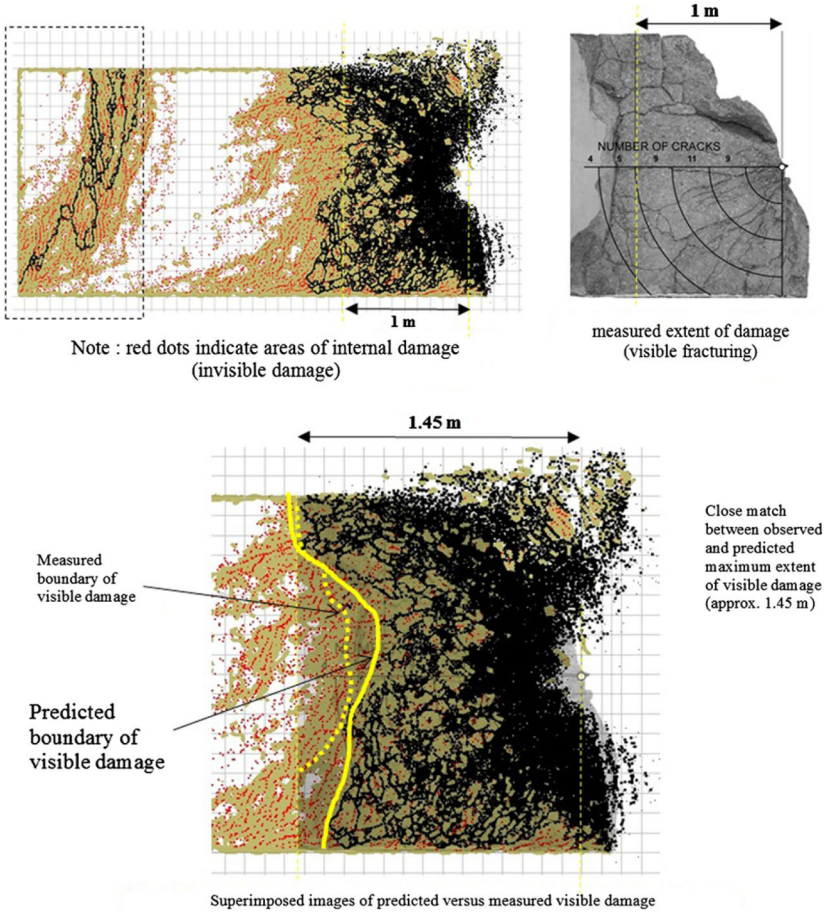

Fig. 12.

Comparison between model predictions and actual measurements for a model section and wire saw cut located 0.3 m from the blast hole collar.

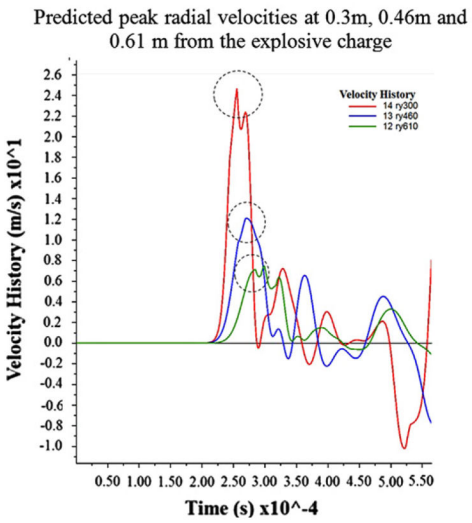

Distance from charge (m)	Measured (m/s)	Predicted (m/s)	Relative Difference %
0.3	25.1	24.7	1.59
0.46	9.88	12.1	-22.4
0.61	4.9	7.0	-42.9

Fig. 13.

Peak radial velocity histories predicted by the HSBM model together with peak radial values measured in the stage 2 concrete block test.

Table 1

Physical properties of concrete block (calibration test).

σ_c (MPa)	T (MPa)	ρ (kg/m^3)	E (GPa)	ν_d
21	1.8	2009	13.1	0.25

σ_C: uniaxial compressive strength; T: tensile strength; ρ: Density; E: static Young's modulus; ν_d: Poisson's ratio.

Table 2

Physical properties of concrete block (validation test).

σ_c (MPa)	T (MPa)	ρ (kg/m^3)	E (GPa)	ν_d
42	2.8	2270	29.5	0.25

σ_C: uniaxial compressive strength; T: tensile strength; ρ: Density; E: static Young's modulus; ν_d: Poisson's ratio.